HIGH FIDELITY MODELING OF ACOUSTIC LINERS FOR AERONAUTICAL APPLICATIONS

Lorenzo Pinelli[1], Michele Marconcini[1], Andrea Arnone[1] & David Bacci[2]

[1]Department of Industrial Engineering, University of Florence, Via S. Marta 3, 50139 Florence, Italy
[2]Oxford Thermofluids Institute, University of Oxford, OX2 0ES, Oxford, United Kingdom

Abstract

Aircraft noise is a polluting emission from civil aviation and is the most significant cause of adverse community reactions related to the operation and expansion of airports. Reducing the population affected by significant aircraft noise is therefore a key priority for aircraft-engine designers. Acoustic liners are a well-established technology to decrease noise emissions and they have been installed in the engine intake and turbine nozzle for a long time. Such passive devices are usually designed to absorb a target band of the noise spectrum radiated from the aft and rear parts of the engine. Liner panels based on single-degree-of-freedom cavities are usually designed using semi-analytical methods and verified with experimental campaigns in dedicated grazing tube rigs. Thanks to the growth in computational capability, high-fidelity simulations of such devices are becoming viable and can be used instead of expensive experimental campaigns. This is particularly true when screening non-conventional geometries of the resonator cavity as Triply Periodic Minimal Surface (TPMS). In this context, the paper presents and validates a high-fidelity numerical approach based on the OpenFOAM open-source CFD code to predict the acoustic impedance and absorption of liner panels. LES simulations of a single resonator cell have been performed with and without grazing flow for different Sound Pressure Level (SPL) of the planar acoustic waves to investigate linear and non-linear regimes of the resonator. Liner impedance and absorption coefficients have been derived by mean of the well-known in-situ method.

Keywords: Computational aeroacoustics (CAA), aircraft noise, acoustic liner

1. Introduction

Nowadays, the recovery of civil air traffic to pre-pandemic standards has brought with it a sharp growth of noise pollution from aviation. Noise pollution is extremely annoying when aircraft are close to the ground (e.g., takeoff, cutback and approach conditions) and noise radiated from the engines and the airframe directly strikes people living near large airports. For this reason, all the modern propulsion systems based on ultra-high bypass ratio turbofan engines must be designed following low-noise design criteria and using more and more accurate acoustic prediction methods [1, 2]. This means that radiated noise from a turbofan engine must be properly abated to comply with international restrictions on the maximum allowable noise emission levels, as indicated by the Flightpath 2050 document [3]. To tackle this issue, acoustic liners have been installed on intake ducts or engine nozzles for a long time. Such passive devices are usually designed to absorb a target band of the noise spectrum radiated from the aft and rear parts of the engine. Acoustic liners attenuate acoustic emissions in a narrow-band frequency range by dissipating acoustic energy into shear stresses and turbulent eddies at the orifices of perforated face sheets. To maximize these viscous effects, the depth of the cavity backing the perforated plate is designed to tune the natural frequency of the Helmholtz resonator with the frequency of the acoustic excitation. In this way, a resonant coupling between the system and the excitation is obtained leading to a non-linear regime of the cross-flow jet oscillations. Following a mechanical analogy, such a system can be sketched as a lumped Single-Degree of Freedom (SDOF) mass-spring-damper, characterized by a single resonant frequency.

From an engineering point of view, the attenuation performed by acoustic liners can be derived from the acoustic impedance of the perforated panel. In other words, under the hypothesis of locally reacting liners, the resonators can be modelled as lumped systems characterized by an acoustic impedance, mimicking an electrical analogy. The most common and practical way to measure the acoustic impedance of SDOF liners is based on the use of one experimental two-microphone technique as described by Dean [4].
However, despite the more and more accurate theoretical models and experimental measurement techniques, none of these approaches can provide a deeper insight into the physical phenomena that lead to the noise abatement of a liner element. To fill this gap, high-fidelity CFD simulations are becoming a viable alternative although only a few works on this topic are already available in literature. A detailed literature review on the acoustic liner modelling strategies (analytical, mid-fidelity and high-fidelity) can be found in the work of Winkler et al. [5] where past practices and future needs are clearly described highlighting the pros. and cons. of the available methodologies. Some of the recent works are based on computational aeroacoustics (CAA) methods [6, 7], Lattice Boltzmann Method (LBM) [8, 9, 10] and Large Eddy Simulations (LES) [11]. Among them, high-fidelity numerical investigations for impedance reduction of a single-element SDOF liner have been carried out by Bodony and Zhang [12]. Through a Direct Numerical Simulation (DNS) approach, they investigated the acoustic response of both single- and multi-orifice perforated plates backed by a hexagonal cavity under no grazing flow and normal incidence of an incoming tonal excitation. The authors further extended their investigation to the single-orifice SDOF liner in the presence of a grazing flow [13] generating a wide DNS database used in this work for validation purposes. A LES approach has been also used by Bauerheim and Joly to investigate the liner aeroacoustic coupling under grazing flow conditions [14], and by Esnault et al. to study synthetic jets in combustor liners [15].
To extend the knowledge about the physics involved in the noise reduction mechanisms of SDOF acoustic liners through high-fidelity simulations, the present paper validates a LES approach to evaluate the acoustic impedance of liner elements for acoustic grazing waves both in the absence and presence of a grazing flow. The geometry of the multi-orifice liner elements is the one experimentally studied by Jones in [16]. The work is focused on the evaluation of the acoustic abatement of these liner elements in a wide range of acoustic wave amplitudes and frequencies, combined with the effect of a grazing flow Mach number (e.g. M = 0.3, M = 0.5). The validation of the LES setup has been achieved by comparing the acoustic performance of multi-orifice cells with a porosity close to Jones' test case against experimental and analytical predictions. To this purpose, the semi-analytical model of Hersh et al. [17] has been used. Furthermore, special attention has been paid to discussing the complex aerodynamic flow structures at the orifice neck strictly linked to noise attenuation.
Finally, as a side objective of the paper it has been demonstrated that high-fidelity approaches are becoming a viable alternative also for liner design, contrasting the historical inertia of using empirically-based tools. This is particularly true for innovative liner concepts (e.g. triply periodic minimal surfaces, TPMS [5]) that might be needed to achieve a lower and broader noise attenuation with more compact configurations. The present study is part of a broad research activity on aircraft engine noise which includes previous studies by the authors on both tonal [18], core noise [19, 20] of aeronautical turbine modules, and on acoustic liner [21].

2. Liner test case

The liner geometry selected for the LES model validation, was the one experimentally studied by Jones et al. at the NASA Langley Research [16] in the test rig named Grazing Flow Incidence Tube (GFIT). Experimental campaigns on impedance reduction of aeronautical liners with and without grazing flow have been carried out by the NASA Langley Research Center Liner Physics Group for a long time [22]. This experimental research activity made available to the aeroacoustic community a large database of high-quality impedance data for different panel configurations extremely useful to validate analytical impedance models and, more recently, high-fidelity (LES, DNS, LBM) computation setups. The original GFIT test rig was continuously improved by implementing different acquisition systems based on the traversing bar (GFIT-TB) and 95 fixed-located microphones (GFIT-95M). All

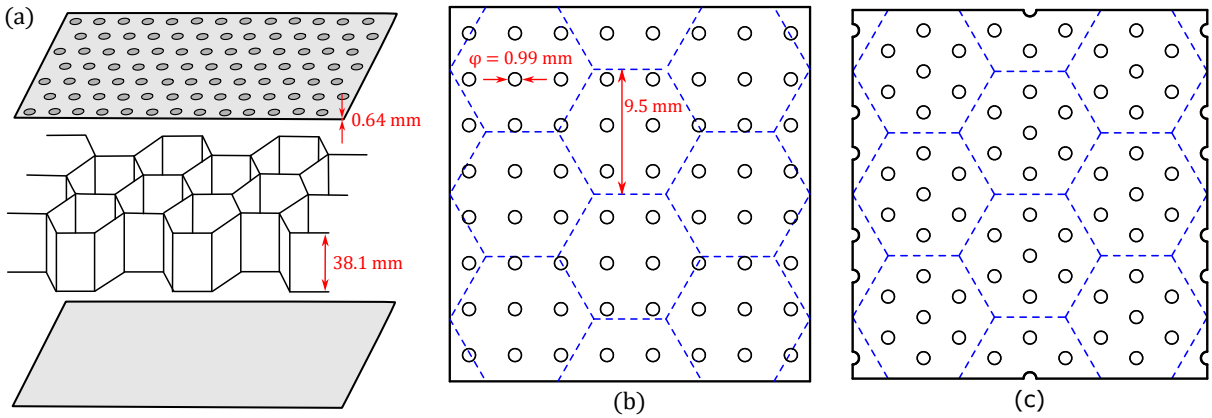

Figure 1 – Schematic of perforated patterns: (a) and (b) conventional liner #1 tested in [16] and (c) the seven-orifices configuration.

the details about the test rig, the impedance test section and the acquisition system can be found in [16].
From pressure signals acquired with microphones, the liner impedance is reduced with both an analytical approach and a 2D finite element method. Different types of acoustic liners, ceramic tubular and two conventional perforated configurations with different porosity, were experimentally studied.
The presented numerical investigation was focused on conventional perforated configuration #1 (low porosity) reported in [16] that is representative of those currently installed inside commercial aircraft engines for noise suppression. The conventional perforated liner configuration #1 consists of an aluminium face sheet bonded onto 9.5 mm diameter hex-cell honeycomb cavities that are 38.1 mm deep. The face-sheet thickness is 0.64 mm, the hole diameter is $\varphi = 0.99$ mm, and the hole density was selected to achieve a porosity $\sigma = 6.4\%$ as shown in Fig. 1(a) and Fig. 1(b). To numerically investigate this configuration with a repetitive pattern, a seven-orifice pattern for each honeycomb cavity configuration was built (see Fig. 1(c)). The diameter of the orifices and hexagon dimensions were kept the same leading to a porosity $\sigma = 6.93\%$, very close to the experimental value.

3. Computational Framework

High-fidelity LES were performed for the three test cases using the open-source OpenFOAM suite [23]. The acoustic response of the multi-orifice SDOF resonator was investigated by varying the excitation frequency (for 500 to 3000 Hz), the SPL (from 120 to 160 dB) and the grazing flow Mach number (0.3 and 0.5). For the latter cases, a uniform laminar inflow was set on the upper box domain. This is an important aspect of the grazing flow simulations as the boundary layer characteristic (laminar or turbulent) has a strong influence on the resistance prediction, as it will be shown later on in the following.

3.1 Domain discretization

The multi-block structured democratization was obtained by using the open-source SALOME software [24]. The entire domain consists of the hexagonal resonator and an upper box where planar acoustic waves are enforced to travel stream-wise. To prevent any interaction between the cross-flow jets and the far-field, the upper box was sized to span a length of 240 orifice diameters in the stream-wise direction (L_x), a height of 100 orifice diameters in the wall-normal direction (L_y) and a width of 80 diameters in the span-wise direction (L_z). An illustration of the numerical domain, and its boundaries is reported in Fig. 2. With regard to the meshing procedure, local grid refinements are needed close to the orifices where complex flow structures are generated by the pulsating jets, especially at the non-linear regimes (e.g. high SPLs or close to resonance). Moving to the orifices region both from the upper domain box and the cavity, the mesh elements are kept as uniform as possible to increase the numerical stability of the simulations. Namely, it is well known that a steep variation in the elements' size or a bad mesh quality in the region of interest might result in a less robust setup. Moreover, the mesh is intentionally coarsened toward the far field regions to reduce the

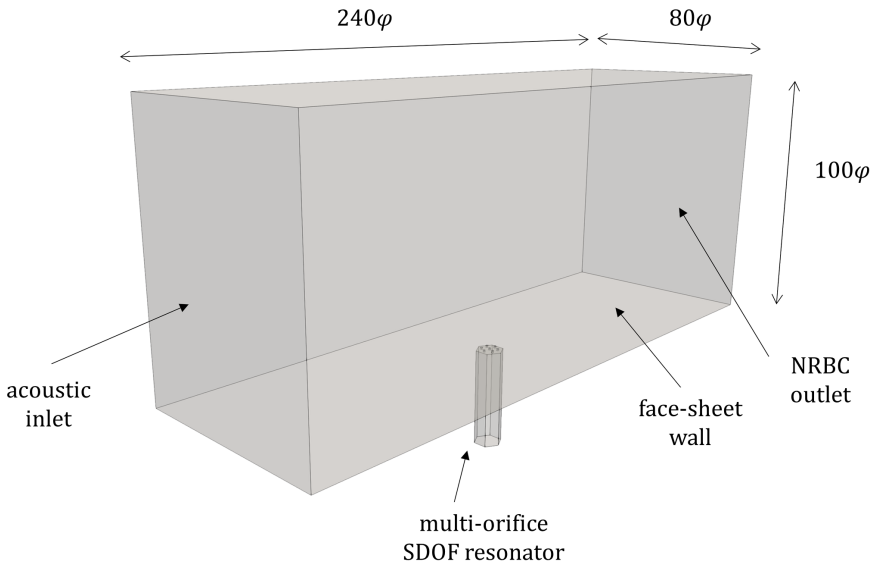

Figure 2 – LES numerical domain: boundaries and dimension related to the orifice diameter.

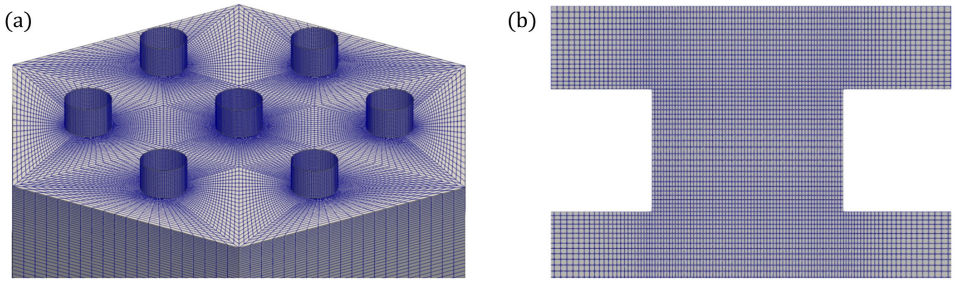

Figure 3 – Mesh detail: orifice region mesh (left), and single-orifice discretization (right)

computational cost. In this way, a proper mesh density around the orifices is achieved, still reducing the total number of elements of the final mesh. To accurately predict the flow oscillations across the orifices and the wall shear stresses, each orifice is discretized by 60 grid points along the diameter. An outward radial refinement was used to stretch the cells down to the orifice lateral surface, resulting in a first off-the-wall cell height of about 0.013 mm. In addition, wall-normal and span-wise mesh refinements are enforced on the upper box to correctly match the coarse mesh in the far-field with the fine one near the orifices. Details of the mesh close to the orifices are shown in Fig. 3. The main meshing parameters are listed in Table 1

3.2 Boundary conditions

In each simulation, a single-frequency planar acoustic wave is forced to travel along the grazing flow direction from the inlet to the outlet of the upper box domain. This is the main difference compared to the analyses presented in [12] where the acoustic wave enters the domain from the domain top. No discrepancies in the acoustic results are expected, and in addition, a grazing acoustic wave is

Total number of elements	8.5×10^6
Mesh points per diameter	60
Minimum number of points per wavelength	40
First cell height at wall [mm]	0.023
Max. average y^+	0.93
Max. aspect ratio	66
Max. cell non-orthogonality	42°

Table 1 – Meshing parameters of the TDOF test-case.

considered more representative of liner panel working conditions in turbofan engines. A sinusoidal variation of the inlet pressure, that generates the planar wave, was specified at the inlet plane through the *uniformFixedValue* boundary condition available in OpenFOAM. This latter set the amplitude and the frequency of the incoming acoustic wave together with the mean pressure on which the acoustic signal superimposes. A non-reflective boundary condition (NRBC) is applied to the outlet boundary to prevent any spurious reflections. This ensured that the acoustic field close to the resonator neck was not altered by spurious boundary effects. To this purpose, the non-reflective *waveTransmissive* boundary condition was selected for all the flow variables transported by the wave equation (e.g. velocity, pressure and temperature). As explained by Poinsot and Lelef [25], such a Robin-type boundary condition solves the inviscid Navier-Stokes equations recast in the characteristics form on the outlet plane. Moreover, the reflectivity of the outlet was adjusted by tuning a stiffness constant which acts as a source term in the in-homogeneous inviscid Navier-Stokes equations. The value of this constant is a measure of how far downstream of the outlet the mean pressure field is. According to the OpenFOAM nomenclature, a value of the L_{inf} parameter equal to 20 was enough to ensure that the grazing acoustic wave left the domain through the outlet without generating any spurious reflections. The standard *noSlip* condition was applied to the velocity field at the resistive plate, while the *cyclicAMI* condition was used to enforce a span-wise periodicity of the flow variables on the upper box. Finally, a uniform temperature of 300 K was specified at the inlet, while walls were treated as adiabatic through the *zeroGradient* boundary condition. A summary of the selected boundary conditions is shown in Table 2.

Boundary	Pressure	Velocity	Temperature
Inlet	*uniformFixedValue*	*zeroGradient*	*fixedValue*
Outlet	*waveTransmissive*	*waveTransmissive*	*waveTransmissive*
Top	*zeroGradient*	*zeroGradient*	*zeroGradient*
Lateral	*cyclicAMI*	*cyclicAMI*	*cyclicAMI*
Walls	*zeroGradient*	*noSlip*	*zeroGradient*

Table 2 – Boundary conditions matrix used for all the test-cases.

3.3 Numerical solver and schemes

The unsteady compressible pressure-based $rhoPimpleFoam$ solver was selected to run the LES. The solver implements the PIMPLE algorithm, which blends the SIMPLE (Semi-Implicit Method for Pressure Linked Equations) [26] and the PISO (Pressure Implicit with Splitting Operator) [27] algorithms to enhance the stability of the time-accurate calculations. After a sensitivity analysis, it was found that two loops on the pressure equation (PISO algorithm) and three pressure-velocity coupling loops (SIMPLE algorithm) were a reasonable trade-off between stability and convergence acceleration requirements. For temporal discretization of the Navier-Stokes equations, an implicit second-order $backward$ scheme was selected. The gradient, the convective, and the diffusive terms were discretized through a blended $Gauss\ localBlended$ scheme. This latter was set to switch between a fourth-order cell-centered $Gauss\ cubic$ scheme close to the orifices and the face-sheet and a first-order upwind $Gauss\ upwind$ scheme far from the line element. This choice was motivated by the need for having high accuracy where pulsating jets and the grazing boundary layer occur while improving the setup stability otherwise. Finally, the Wall-Adapting Local Eddy-Viscosity (WALE) sub-grid model was selected to close the system of Navier-Stokes equations.

All the simulations were run until reaching the convergence of acoustic pressure inside the resonator by using 160 cores of a Linux cluster equipped with Intel CPU E5-2680 at 2.8 GHz, taking from 24 to 96 hours to obtain a converged and periodic solution. The statistical convergence of the solution was monitored by recording the pressure signal at the cavity back wall. More precisely, the duration of the acoustic transient was defined as the time the acoustic oscillations inside the resonator need to reach a constant amplitude. Depending on the characteristic of the excitation, this time ranged from 20 to 50 periods of the acoustic forcing. The time step adopted for each simulation was kept tight enough to accurately reproduce the incoming wave, preventing undesirable aliasing. At the same time, the

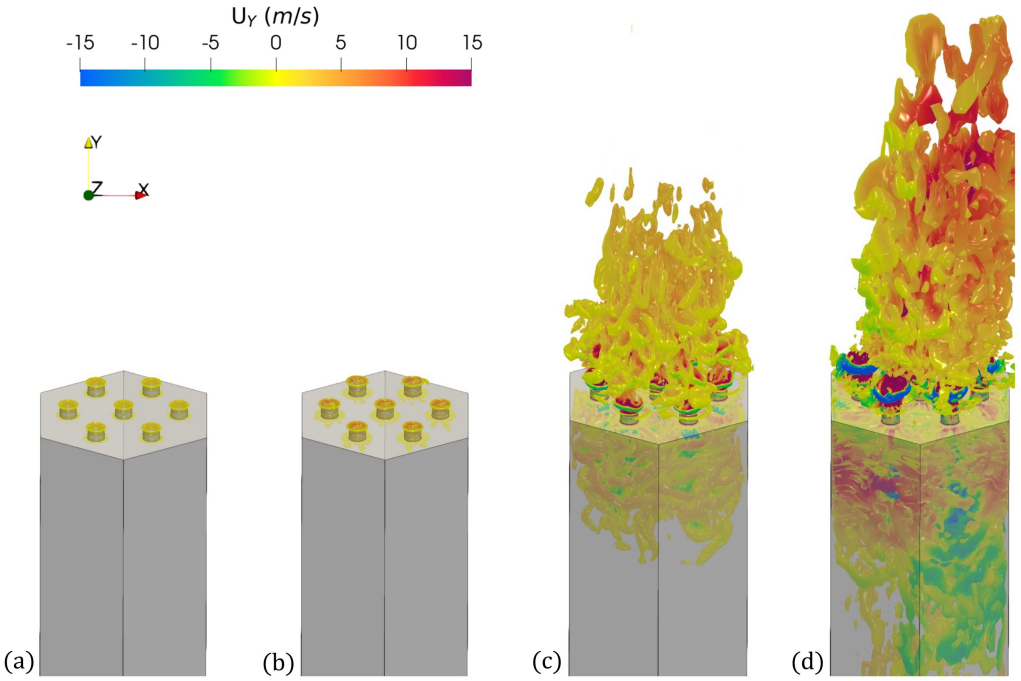

Figure 4 – Q-criterion at different SPLs - multi orifice: : (a) 130 dB; (b) 140 dB; (c) 150 dB and (d) 160 dB.

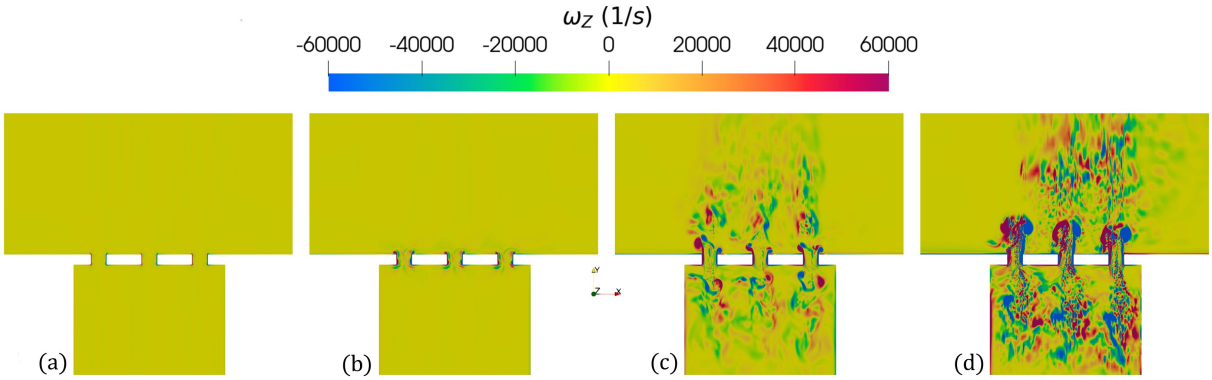

Figure 5 – Spanwise vorticity contours - multi orifice: : (a) 130 dB; (b) 140 dB; (c) 150 dB and (d) 160 dB.

Courant-Friedrich-Lewy constraint $CFL_{max} < 1$ was satisfied everywhere in the domain even for the grazing flow calculations. This led to a reduction of the dimensional time-step from 1 μs (used for the no grazing flow cases) to 20 ns for the grazing flow analysis with the highest Mach number (M = 0.5).

4. Result and discussion

4.1 Acoustic-induced flows at the orifices

Non-linear oscillations of the cross-flow jets are expected when liners operate at high SPLs or close to a resonant frequency. Although the highest noise suppression is observed only in the case of resonance, the non-linear response of the system can be qualitatively evaluated from the shape of the pulsating jets driven by the acoustic excitation. For this reason, the present section discusses the characterization of the turbulent structures solved by the LES approach when non-linear jet oscillations occur.

Q-criterion contours coloured with the cross-flow jet velocity are displayed in Fig. 4 for different levels of acoustic excitation. To help detect the main flow features at the orifice region, spanwise vorticity contours are plotted on the cell mid-plane as well (see Fig. 5). It is well clear that the transition to a fully non-linear regime occurs when the acoustic excitation amplitude is above 140 dB. Below this

threshold, the 3 kHz acoustic forcing on the orifice section generates very low jet oscillations. No major turbulent structures arise under this amplitude and the linearity of the jet oscillations can be assumed. On the other hand, when the amplitude increases over 140 dB, the jet starts to penetrate more into the cavity and the upper domain box, progressively losing its original cylindrical shape. More in detail, when the oscillation regime becomes highly non-linear (e.g. 150 dB), some coherent and toroidal structures are generated at the orifice rim. At the same time, the potential jet core starts to shrink and two viscous low-speed boundary regions become visible on the orifice walls. These effects are magnified at the amplitude of 160 dB when the jet oscillations are so intense to determine the breakdown of the coherent turbulence. In other words, the higher the incoming acoustic energy is, the smaller and more energy-carrying eddies detach from the orifice. This also leads to a more evident wrinkling of the external jet surface which becomes highly irregular. The asymmetry of the jet structures, at highly non-linear regimes, are due to the presence of the grazing acoustic wave that propagates from left to right in all the visualizations.

4.2 Impedance eduction

In this section, the impedance evaluation of the test case under investigation is reported. The results from the LES of the multi-orifice single-cavity cell are compared with the experiments of Jones [16] and the semi-empirical model of Hersh [28] to validate the LES setup on a realistic liner pattern. For the grazing flow cases, the authors have also compared their results with the numerical analysis conducted by Zhang and Bodony [13].
Before showing the numerical results, the experimental two-microphone methods proposed by Dean [4] for impedance evaluation must be illustrated. These techniques have been implemented into the OpenFOAM environment by including virtual microphones to derive the acoustic impedance from the LES results. The sketch of the two–microphone in-situ methods is shown in Fig. 6.

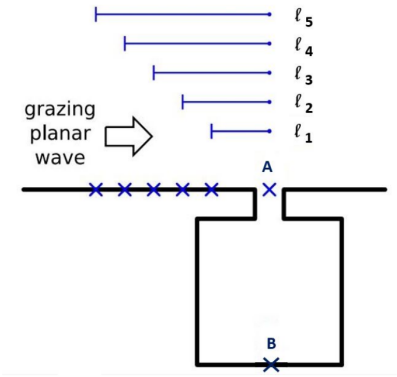

Figure 6 – Probe array for the in-situ method application: (a) SDOF, (b) TDOF.

Mimicking an experimental rig, the acoustic signals were recorded by virtual pressure probes, at the cavity back-wall (B) and at the face-sheet centre-line, upstream of the orifice aperture (A), as shown by Fig. 6. Since these in-situ techniques might suffer from the hydrodynamic influence of the pulsating jets, a set of five probes aligned with the face-sheet centre-line was considered. The upstream distances at which the face-sheet probes were placed are respectively: $\ell_1 = 6d$, $\ell_2 = 12d$, $\ell_3 = 18d$, $\ell_4 = 24d$, $\ell_5 = 30d$, being d the orifice diameter. The pressure signals are then processed by a DFT algorithm to derive the specific acoustic impedance of the liner element by using Eq. 1.

$$z(\omega) = -j\frac{|p_A|}{|p_B|}\frac{e^{j\Phi_{AB}}}{sin(kL)} \tag{1}$$

In the above expressions, L is the cavity depth, k is the acoustic wave number, Φ is the phase shifting between the face-sheet and the cavity pressure signals, and P_i is the complex pressure amplitudes. Since from an experimental point of view, it is unfeasible to place a microphone exactly at the orifice aperture, the acoustic pressure in A was reconstructed from the signal recorded by one of the face-sheet probes at position A_i. More precisely, knowing the linear distance ℓ_i between the face-sheet

probe and the orifice aperture, the grazing flow Mach number M and the excitation wavelength λ, the phase shift Φ_{AiA} between the acoustic signal at the probe and the orifice aperture is given by:

$$\Phi_{A_iA} = \frac{2\pi\ell_i}{\lambda(1+M)} \tag{2}$$

Finally the phase shift Φ_{AB} in Eq. 1 is retrieved by subtracting the translation term Φ_{AiA} to the acquired phase shift Φ_{AiB}.

4.2.1 No-flow condition

The trends of the acoustic resistance and reactance for a 130 dB acoustic excitation are shown in Fig. 7. Here, the frequency response predicted by the LES is represented by the black squares. The results coming from the semi-analytical Hersh model are represented by the red dashed line, while the light-blue circles and the blue pentagons come from Jones' acquisitions.

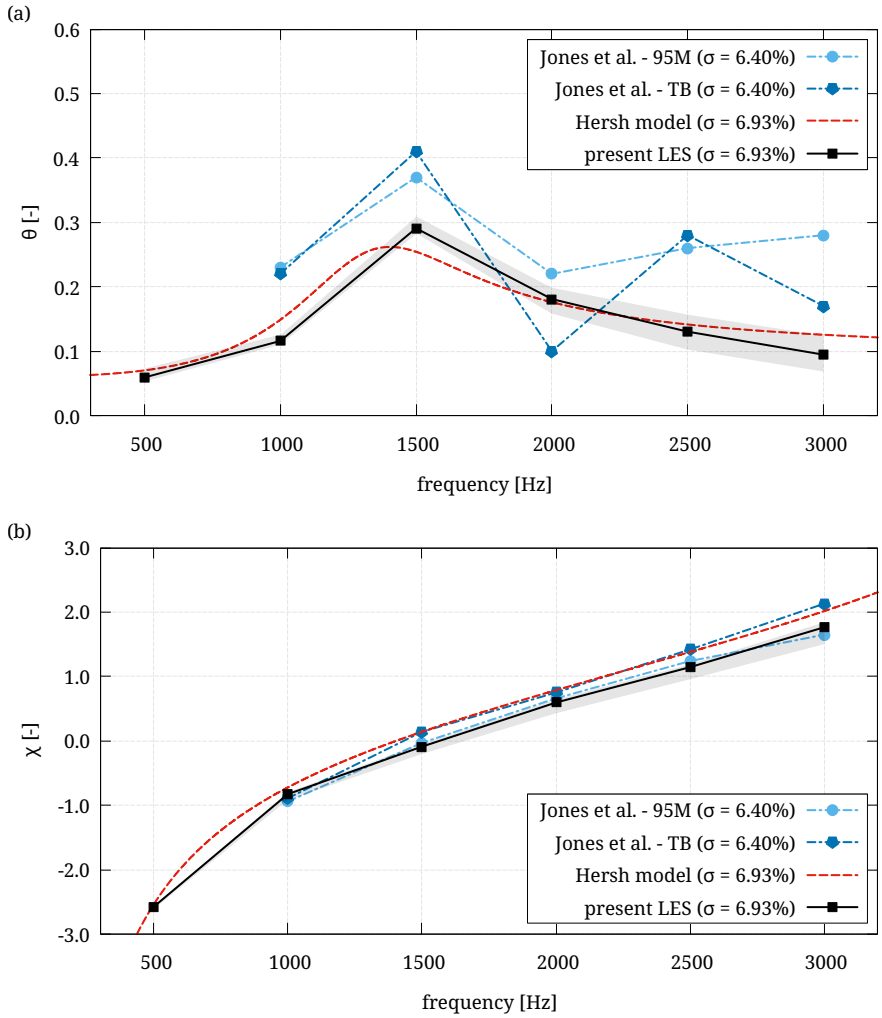

Figure 7 – Specific resistance (a) and reactance (b) at fixed 130 dB SPL.

As shown in Fig. 7, a good agreement between the LES results and the Hersh model is found for both the resistance and the reactance over the entire frequency range. To collapse LES impedance evaluations coming from the different probe A_i locations into a single black square an average on the face-sheet probe results has been used. Moreover, the shaded bandwidth across the black squares indicates the range of variation of the resistance and the reactance at each frequency. Looking at the experiments from Jones, it can be noted that the LES correctly matches the resistance peak at around 1.5 kHz which is predicted also by the Hersh model but at a slightly lower frequency. At the same time, the anticipation of the reactance zero-crossing means that the Hersh model underestimates the resonant frequency at about 1.3 kHz. This discrepancy may come from the approximation of the

seven-orifice perforation pattern with an equivalent single orifice with the same opening area. This assumption has been made as in the Hersh model formulation, a unique value for the discharge coefficient for a single hole was considered when implementing the formula to obtain the analytical resistance. Conversely, a marked mismatch between experiments and the LES results is visible for frequencies higher than the resonant one. Here the LES follows the trend of the Hersh model but it keeps decreasing instead of showing a secondary peak around 2.5 kHz. It should be noted that the two experimental techniques (i.e., 95 microphones and traversing bar) used by Jones gave different results on the same liner geometry for frequencies higher than 1.5 kHz. Furthermore, the authors consider the 95 microphone measurement the most reliable one, as it is not well clear why a secondary peak coming from the traversing bar method should appear in a locally reacting SDOF system. On the other hand, it should be considered that the porosity of the liner tested by Jones is not the same as the one of the liner investigated by using the LES and the Hersh approaches. Since the liner porosity enters mainly into acoustic resistance evaluation, this might explain why greater deviations have been found on resistance, while reactance values have been predicted in an excellent agreement among all the three approaches.
Moving now to SPL effects, in Fig. 8 the acoustic quantities are plotted against the SPL for an excitation frequency equal to 3 kHz. In this case, the LES results are only compared with the Hersh model due to the lack of experiments at SPLs higher than 130 dB. From Fig. 8 it can be observed

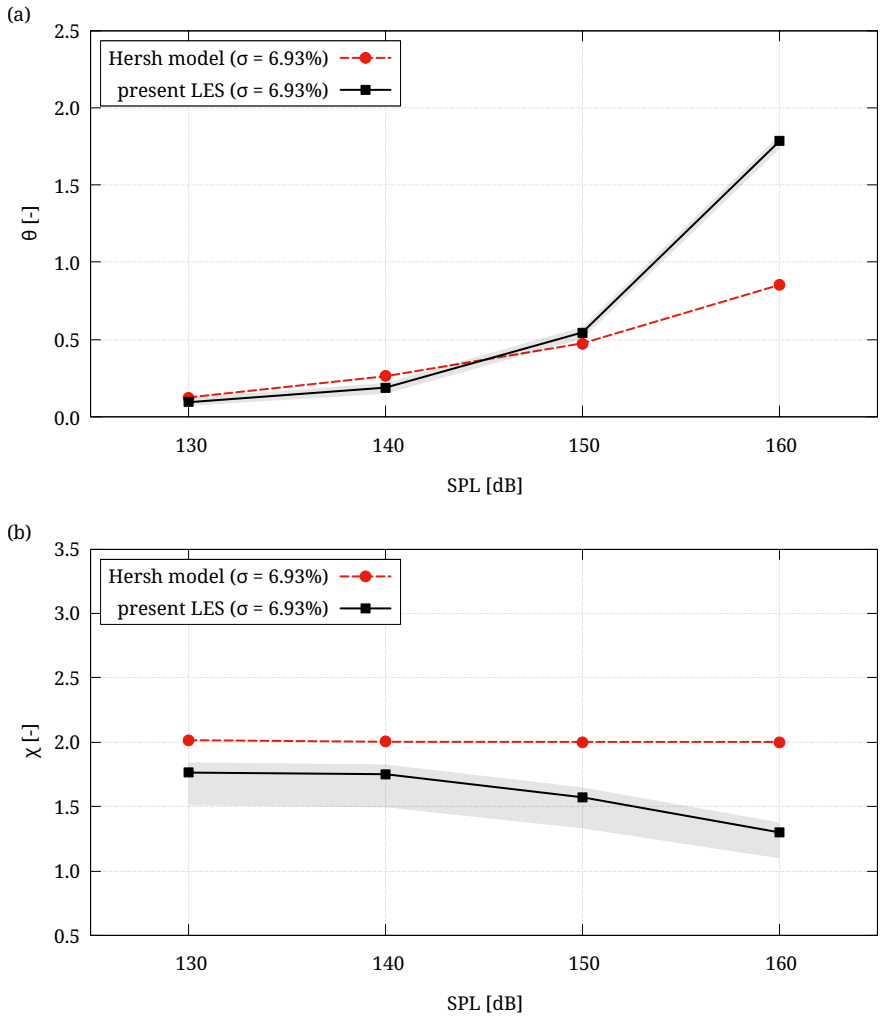

Figure 8 – Specific resistance (a) and reactance (b) at fixed 3 kHz frequency.

that the sensitivity to the face-sheet probe location (grey band) affects the reactance estimation more than the resistance one. Moreover, almost no effect of the SPL has been found on the bandwidth thickness meaning that the in-situ method of Dean is marginally influenced by the oscillation regime. Focusing on Fig. 8(a), the numerical and the analytical resistance predictions agree well up to 150

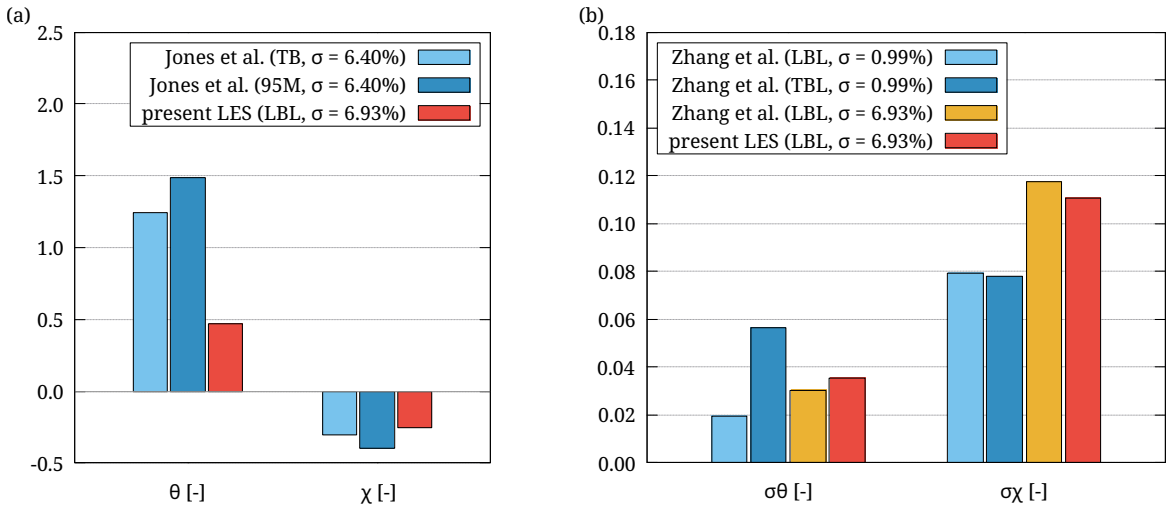

Figure 9 – Effect of the grazing flow boundary layer on resistance and reactance: M = 0.3, f = 1.5 kHz (a); M = 0.5, f = 3.0 kHz (b).

dB. From this threshold on, an abrupt increase in the resistance is predicted by the LES so that at 160 dB the numerical resistance nearly doubles the analytical prediction. The reason behind this discrepancy is probably due to the lack of cross-flow contribution when deriving the discharge coefficient through the Hersh model. More in detail, it can be deduced that the acoustic discharge coefficient coming from the LES simulation at 160 dB and 3 kHz is lower than the one computed in the analytical model. Since a lower discharge coefficient value implies a greater blockage on the orifice walls, the increase in acoustic resistance for the LES simulation is thus motivated. On the other hand, at the quasi-linear regimes, the jets' oscillation is damped, thus reducing the hydrodynamic contribution to the overall discharge coefficient. As a result, a closer match between the Hersh model and the LES has been found at lower SPLs. Focusing now on the reactance, the Hersh model predicts an almost constant reactance at all the investigated SPLs whereas a decreasing trend can be observed for the LES simulations. This is again due to the way the Hersh model computes the discharge coefficient at very high SPLs. According to the model implementation [28], the frequency dependency of the discharge coefficient is unaltered when a fully non-linear behaviour of the acoustic system holds. This means that from a certain threshold on, the increasing SPL affects no more the resonator inertial length, leading to a constant reactance as shown by Fig. 8(b). Actually, as the discharge coefficient keeps decreasing, a further reduction of the inertial length is expected, thus leading to a decreasing reactance as well. In other words, it can be concluded that from the Hersh model, almost the same amount of non-linearity is predicted for SPLs ranging from 130 dB to 160 dB. Conversely, the LES shows a tendency towards a quasi-linear response for SPLs equal to 130 dB or 140 dB, locating the fully non-linearity threshold beyond 150 dB. The difference between the numerical and the analytical approaches might lie once again in the reduction of the seven-orifice pattern to an equivalent single-orifice configuration when applying the Hersh model. More in detail, the number of orifices and the perforation pattern may determine conjugate interactions between the pulsating jets that are not modelled by the analytical approach.

4.2.2 The grazing-flow condition

For the grazing flow cases, LES results have been compared with the numerical results from Zhang and Bodony [13] and the experiments of Jones [16] separately. More precisely, an excitation at 1.5 kHz was superimposed at M = 0.3 grazing flow Mach number to recreate the experiments of Jones, while a 3.0 kHz excitation with M = 0.5 grazing flow Mach number was selected to replicate the DNS of Zhang and Bodony [13].

Looking at Fig. 9(a) it can be seen that the present LES calculations strongly underestimate acoustic resistance when compared to the experiments. This is due to the laminar boundary layer of the grazing flow at the face-sheet holes in the upper box of the numerical domain. It should be recalled that in

the LES setup, no turbulent inflow was provided at the domain inlet and the upstream distance is not enough to cause the boundary layer transition that is triggered downstream the holes by the pulsating jet. The effect of the laminar boundary layer is evident also from Fig. 9(b), where the comparisons with Zhang and Bodony [13] of the acoustic quantities are reported. In their work, Zhang and Bodony who imposed both laminar and turbulent boundary layers, stressed that the normalized acoustic resistance σ θ is expected almost to triple if a turbulent inflow is specified (see the resistance bars in Fig. 9(b)). This was demonstrated for a single-orifice liner but it can be reasonably derived that the same is true for any perforation pattern. Indeed, the bars referred to the seven-orifice configuration under a laminar grazing flow are in good agreement in terms of acoustic resistance. This is further proof of the influence of the boundary layer characteristic on the liner performance. The explanation for this evidence lies in the amount of energy carried by a laminar and turbulent boundary layer. It is known that turbulent transition makes the boundary layer more energized so a higher acoustic energy is required to make the jet penetrate the boundary layer over the orifices. As a consequence, this means that turbulent boundary layers hamper the feeding of resonators due to the incoming forcing, leading to an increase in the acoustic resistance.

5. Conclusions

The paper presents a wide numerical investigation of acoustic liners for aeronautical applications. The first aim of the authors has been the validation of a proposed LES approach for the impedance reduction of a realistic multi-perforated liner against experimental data. The acoustic impedance of Jones's test case without grazing flow conditions has been predicted for different amplitudes and frequencies of the acoustic excitation. Some additional, and more computationally expensive simulations, have been also carried out to prove the reliability of the presented LES approach under realistic grazing flow conditions. The LES results have been compared with both experimental data and analytical predictions and demonstrated the robustness and accuracy of the LES approach. An excellent agreement between the LES and the analytical predictions has been found, both in terms of acoustic resistance and reactance. At the same time, some discrepancies have been outlined when comparing the LES results with the experimental acquisitions, mainly for the excitation frequencies around 2500-3000 Hz. Due to the lack of experimental data at SPLs larger than 130 dB, the acoustic performance at very non-linear regimes has been evaluated by a LES-to-analytical comparison only. In this comparison, the LES results have been found to overestimate acoustic resistance, especially at SPL = 160 dB. Moreover, a decreasing trend in LES reactance has been observed, while the analytical method did not reveal any dependency of the acoustic reactance on increasing SPL. The influence of a grazing flow on the acoustic response of the resonator has been also compared, and it has been concluded that it is mandatory to include a turbulent boundary layer in the LES environment to correctly capture the acoustic resistance increase at the high-speed grazing flows. Furthermore, as a side result, the LES results have allowed an accurate characterization of the pulsating jets, highlighting the complex mechanisms that lead to noise abatement.

6. Acknowledgments

The authors from University of Florence acknowledge the contribution of Sustainable Mobility Center (Centro Nazionale per la Mobilità Sostenibile - MOST), funded by European Union – NextGenerationEU (CUP B13C22001000001).

7. Contact Author Email Address

Contact author: Lorenzo Pinelli (lorenzo.pinelli@unifi.it)

8. Copyright Statement

References

[1] Stéphane Moreau. Turbomachinery noise predictions: Present and future. *Acoustics*, 1(1):92–116, 2019, doi:https://doi.org/10.3390/acoustics1010008.

[2] Attila Balázs Nagy, Jan Delfs, and Gareth J. Bennett. Aeroacoustics research in europe: The ceas-asc report on 2020 & 2021 highlights. *Journal of Sound and Vibration*, 534:117002, 2022, doi:https://doi.org/10.1016/j.jsv.2022.117002.

[3] European Commission, Directorate-General for Mobility, Transport, Directorate General for Research, and Innovation. *Flightpath 2050 – Europe's vision for aviation – Maintaining global leadership and serving society's needs*. Publications Office, 2011.

[4] Peter D. Dean. An in situ method of wall acoustic impedance measurement in flow ducts. *Journal of Sound and Vibration*, 34(1):97–IN6, 1974, doi:https://doi.org/10.1016/S0022-460X(74)80357-3.

[5] Julian Winkler, Jeffrey M. Mendoza, C. Aaron Reimann, Kenji Homma, and Jose S. Alonso. High fidelity modeling tools for engine liner design and screening of advanced concepts. *International Journal of Aeroacoustics*, 20(5-7):530–560, 2021, doi:10.1177/1475472X211023884.

[6] Christopher K.W. Tam, Nikolai N. Pastouchenko, Michael G. Jones, and Willie R. Watson. Experimental validation of numerical simulations for an acoustic liner in grazing flow: Self-noise and added drag. *Journal of Sound and Vibration*, 333(13):2831–2854, 2014, doi:https://doi.org/10.1016/j.jsv.2014.02.019.

[7] Rémi Roncen, Fabien Méry, Estelle Piot, and Patricia Klotz. Spatially-varying impedance model for locally reacting acoustic liners at a high sound intensity. *Journal of Sound and Vibration*, 524:116741, 2022, doi:https://doi.org/10.1016/j.jsv.2021.116741.

[8] Adrien Mann, Franck Perot, Min-Suk Kim, and Damiano Casalino. Characterization of acoustic liners absorption using a lattice-boltzmann method. In *19th AIAA/CEAS Aeroacoustics Conference*, pages 4032–4052, Berlin, Germany, 27–29 May, 2013. doi:https://doi.org/10.2514/6.2013-2271.

[9] Chenzhen Ji and Dan Zhao. Lattice boltzmann investigation of acoustic damping mechanism and performance of an in-duct circular orifice. *The Journal of the Acoustical Society of America*, 135(6):3243–3251, 2014, doi:https://doi.org/10.1121/1.4876376.

[10] Damiano Casalino, A. Hazir, and Adrien Mann. Turbofan broadband noise prediction using the lattice boltzmann method. *AIAA Journal*, 56(2):609–628, 2018, doi:https://doi.org/10.2514/1.J055674.

[11] Jean Dassé, Simon Mendez, and Franck Nicoud. Large-eddy simulation of the acoustic response of a perforated plate. In *14th AIAA/CEAS Aeroacoustics Conference and Exhibit*, pages 2983–2991, Vancouver, BC, Canada, 5–7 May, 2008. doi:https://doi.org/10.2514/6.2008-3007.

[12] Qi Zhang and Daniel J. Bodony. Numerical investigation and modelling of acoustically excited flow through a circular orifice backed by a hexagonal cavity. *Journal of Fluid Mechanics*, 693:367–401, 2012, doi:https://doi.org/10.1017/jfm.2011.537.

[13] Qi Zhang and Daniel J. Bodony. Numerical investigation of a honeycomb liner grazed by laminar and turbulent boundary layers. *Journal of Fluid Mechanics*, 792:936–980, 2016, doi:https://doi.org/10.1017/jfm.2016.79.

[14] Michaël Bauerheim and Laurent Joly. LES of the aero-acoustic coupling in acoustic liners containing multiple cavities. In *AIAA Aviation 2020 Forum*, page 2571, 2020. doi:https://doi.org/10.2514/6.2020-2571.

[15] Soizic Esnault, Florent Duchaine, Laurent Gicquel, and Stéphane Moreau. Large eddy simulation of heat transfer within a multi-perforation synthetic jets configuration. *Journal of Turbomachinery*, 142(6), 2020, doi:https://doi.org/10.1115/1.4046545.

[16] Michael Jones, Willie Watson, Tony Parrott, and Charles Smith. Design and evaluation of modifications to the nasa langley flow impedance tube. In *10th AIAA/CEAS Aeroacoustics Conference*, page 2837, Manchester, UK, 10-12 May, 2004. doi:https://doi.org/10.2514/6.2004-2837.

[17] Joseph Celano, Alan Hersh, and Bruce Walker. Semi-empirical helmholtz resonator impedance model. In *5th AIAA/CEAS Aeroacoustics Conference*, page 1825, Bellevue, WA, USA, 10-12 May, 1999. doi:https://doi.org/10.2514/6.1999-1825.

[18] Lorenzo Pinelli, Francesco Poli, Michele Marconcini, Andrea Arnone, Ennio Spano, and Davide Torzo. Validation of a 3D linearized method for turbomachinery tone noise analysis. In *Proceedings of the ASME Turbo Expo 2011*, pages 1033–1042, Vancouver, British Columbia, 6-10 June, 2011. doi:https://doi.org/10.1115/GT2011-45886.

[19] Lorenzo Pinelli, Michele Marconcini, Roberto Pacciani, Andrea Notaristefano, and Paolo Gaetani. The Effects of Swirling Flows in Entropy Wave Convection Through High-Pressure Turbine Stage. *Journal of Turbomachinery*, 145(3), 10 2022, doi:https://doi.org/10.1115/1.4055613. 031004.

[20] Lorenzo Pinelli, Michele Marconcini, Roberto Pacciani, Friedrich Bake, Karsten Knobloch, Paolo

Gaetani, and Giacomo Persico. Effect of clocking on entropy noise generation within an aeronautical high pressure turbine stage. *Journal of Sound and Vibration*, 529:116900, 2022, doi:https://doi.org/10.1016/j.jsv.2022.116900.

[21] Simone Giaccherini, Lorenzo Pinelli, Michele Marconcini, Roberto Pacciani, and Andrea Arnone. Validation of an Analytical Model for the Acoustic Impedance Eduction of Multicavity Resonant Liners by a High-Fidelity Large Eddy Simulation Approach. *Journal of Turbomachinery*, 145(8):081002, 04 2023, doi:https://doi.org/10.1115/1.4056984.

[22] Willie R. Watson, Sharon E. Tanner, and Tony L. Parrott. Optimization method for educing variable-impedance liner properties. *AIAA Journal*, 36(1):18–23, 1998, doi:https://doi.org/10.2514/2.369.

[23] Henry G. Weller, Gavin Tabor, Hrvoje Jasak, and Christer Fureby. A tensorial approach to computational continuum mechanics using object-oriented techniques. *Computers in Physics*, 12(6):620–631, 1998.

[24] Andre Ribes and Christian Caremoli. Salomé platform component model for numerical simulation. In *31st Annual International Computer Software and Applications Conference*, volume 2, pages 553–564, Beijing, China, 24-27 July, 2007. doi:https://doi.org/10.1109/COMPSAC.2007.185.

[25] Thierry J. Poinsot and Sanjiva K. Lele. Boundary conditions for direct simulations of compressible viscous flows. *Journal of Computational Physics*, 101(1):104–129, 1992, doi:https://doi.org/10.1016/0021-9991(92)90046-2.

[26] Larry S. Caretto, David Gosman, Suhas V. Patankar, and Brian D. Spalding. Two calculation procedures for steady, three-dimensional flows with recirculation. In *Proceedings of the Third International Conference on Numerical Methods in Fluid Mechanics*, pages 60–68. Springer, Paris, France, 3-7 July, 1973.

[27] Raad I. Issa. Solution of the implicitly discretised fluid flow equations by operator-splitting. *Journal of Computational Physics*, 62(1):40–65, 1986, doi:https://doi.org/10.1016/0021-9991(86)90099-9.

[28] Alan Hersh, Bruce Walker, and Joseph Celano. Effect of grazing flow and SPL on impedance of 2-DOF resonators. In *8th AIAA/CEAS Aeroacoustics Conference*, page 2443, Breckenridge, CO, USA, 17-19 June, 2002. doi:https://doi.org/10.2514/6.2002-2443.